ELSEVIER

Catalysis Today 69 (2001) 183–192

CATALYSIS TODAY

www.elsevier.com/locate/cattod

Design of a microstructured reactor with integrated heat-exchanger for optimum performance of a highly exothermic reaction

E.V. Rebrov, M.H.J.M. de Croon, J.C. Schouten*

Laboratory of Chemical Reactor Engineering, Schuit Institute of Catalysis, Eindhoven University of Technology, PO Box 513, 5600 MB Eindhoven, The Netherlands

Abstract

The activity and the heat transfer characteristics of several microstructured reactors have been compared in the ammonia oxidation on Pt catalyst. The main parameters which influence reactor performance are catalyst loading, temperature, and the intrinsic conductivity of the reactor material. In case of aluminum as a reactor material, hot spot temperatures were within 5°C at full conversion of 6 vol.% NH_3. Temperature gradients were considerably larger when the microreactor was made from pure platinum due to the smaller intrinsic material conductivity. As a result, the maximum N_2O selectivity was by 20% lower than in the case of the aluminum-based reactor due to considerable differences in the selectivities between the central and wall channels. Experimental data obtained on the above microreactors were used to design an externally cooled cross flow microreactor/heat-exchanger operating at almost isothermal conditions even with a reaction mixture corresponding to an adiabatic temperature rise of about 1400°C. Such system can provide new opportunities for improvement of existing gas/solid catalytic processes with strongly exothermic reactions.

Keywords: Microreactor; Partial oxidation; Heat transfer

1. Introduction

Current technology development and commercialization efforts are targeted at fabricating complex chemical systems within the volume of a cubic centimeter [1]. These microchemical components can be assembled into larger system architectures, which can perform desired chemical conversions at desired production rates. Characteristic dimensions of microchannels in the range of 100–500 μm open new possibilities for reaction pathways by achieving previously inaccessible residence times and heat transfer rates. Furthermore, the exothermic reactions can be carried out safer because of decreased risk of flame propagation and more efficient heat removal from the reaction zone [2,3].

The use of structured honeycomb reactors is well established in environmental catalysis [4]. However, only sparse attempts have been reported in the literature concerning their applications to catalytic processes for the production of chemicals [5,6]. In fact, the latter involves at least two great potential advantages over conventional packed-bed reactors, namely, strongly reduced pressure drops and more favorable heat transfer properties due to improved heat conduction in the monolith structure. The question of whether structured reactors with optimized specific design can effect significant reduction of the hot spots in the reactor has been addressed in several studies [7–12]. Some of them demonstrated only slightly improved effective heat transfer characteristics in comparison to packed beds of pellets [7]. However,

* Corresponding author. Tel.: +31-40-2472850; fax: +31-40-2446652.
E-mail address: j.c.schouten@tue.nl (J.C. Schouten).

0920-5861/01/$ – see front matter
PII: S0920-5861(01)00368-6

these results refer to existing commercial supports, which were not originally designed in view of optimal heat conduction properties but were typically selected for their resistance to high temperatures.

Recent experimental studies provide an increased understanding of fluid mechanics and heat transfer on the micro scale [9–11]. The objective of this work is therefore to combine these recent findings in fluid flow dynamics and energy transport with basic knowledge on catalyst preparation to design structured microreactor systems with required properties. The needed structure functions are: a rapid heating of the reaction mixture from ambient to high temperatures, a very fast heat removal rate from the reaction zone to avoid hot spot formation, and a rapid cooling of the reaction products.

In the present work, we studied ammonia oxidation on a Pt catalyst in different types of microchannel architectures which were specially constructed for this investigation. The choice of this oxidation reaction is suggested by the fact that the reaction is strongly exothermic. Therefore, the heat distribution between the catalytic surface and the gas phase along the microchannel is important to obtain a high selectivity to one of the reaction products (N_2, N_2O, NO), as this is strongly dependent on the reactor temperature. Furthermore, the ammonia oxidation reaction is structure sensitive, as the selectivity is also strongly dependent on the Pt dispersion [13].

2. Experimental

2.1. Microstructured reactors

All microstructured reactors were positioned in a specially designed reactor housing shown in Fig. 1. The complete reactor module consists of three parts: the actual microreactor, the furnace, and the cooler. The reactor has a nickel housing with standard tube connections and can be heated up to 430°C with an electrical furnace. The furnace is made of copper and could provide power input up to 185 W. The temperature was measured both inside the furnace (T1) and at an outer surface of the reactor (T2). Another thermocouple is positioned on the outer surface of the cooler (T3). To isolate the cooler section from the microreactor, a 2-mm ceramic ring is positioned between the

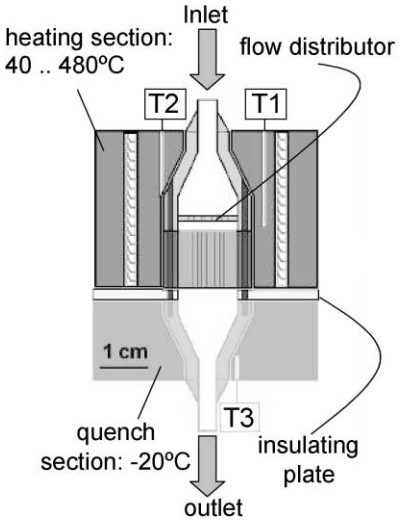

Fig. 1. Microreactor test module consisting of the actual microreactor, the furnace, and the cooler.

microreactor and the cooler. The temperature of the cooler was maintained at about −20°C by a circulating cooling agent in order to provide the fast removal of heat produced in the reactor zone via four stainless steel screws to the cooler. The second use of the cooler is to quench the gas phase reactions and prevent further oxidation of the desired products downstream of the reactor.

Four microstructured reactors were designed and investigated. Three of them (A–C) contain a set of reaction channels of different size and geometry. The reactor D was a combined microreactor/heat-exchanger which was designed and constructed based on the results of experimental studies carried out with reactors A–C and numerical simulation of temperature profiles obtained at higher inlet concentrations of ammonia. The following is a short description of these microstructured reactors.

(A) *Parallel plate reactor*. This microreactor consists of a stack of 20 removable plates, each with a length of 0.7 cm and a width of 0.434 cm. The plates of 0.03 cm thickness are placed at equal distances of 280 micron from each other. The detailed view of this type of microreactor was shown elsewhere [14]. In the present study, the plates were made of aluminum with an alumina layer on both sides produced by anodic oxidation. Platinum was immobilized by wet impregna-

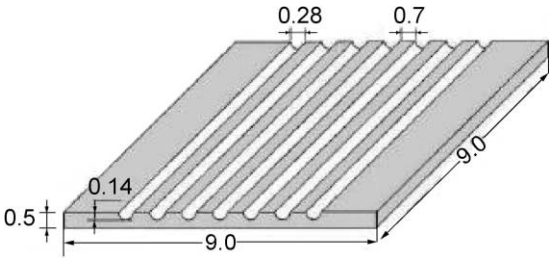

Fig. 2. Schematic view of a single aluminum plate used in the microreactor C. Distances are given in millimeters.

tion of a 1:1 solution of chloroplatinic and citric acids at room temperature for 6 h. The Pt concentration was chosen to provide the desired metal loading of the catalyst. Calcination at 400°C for 6 h, followed by reduction in a hydrogen flow (30 ml/min) for 1 h, was applied to make an active catalyst. To investigate the effect of Pt loading three catalysts with different Pt loading of 0.05, 0.2, and 1.3% wt./wt. Al_2O_3 were prepared. The corresponding parallel plate microreactors are called A1, A2, and A3, respectively.

(B) *Pt-monolith reactor*. This microreactor contains a set of 49 channels of 500 μm in diameter and length of 9 mm produced by conventional machining in a metallic Pt cube with a volume of $10 \times 10 \times 9\,mm^3$. Each row contains seven microchannels positioned at equal distance of 500 μm from each other. The distance between the rows was also 500 μm.

(C) *Assembled Pt/Al_2O_3/Al reactor*. This aluminum microreactor was designed and constructed in order to verify the feasibility of improving the heat transfer properties at the interface between the catalyst plates and the reactor housing. After anodic oxidation, the reactor is assembled from 14 individual plates shown in Fig. 2. Thus, the reactor also contains 49 parallel channels. Pt impregnation was done after reactor assembly with a 1:1 solution of chloroplatinic and citric acids which was circulated through the reactor channels at room temperature for 6 h. To obtain an even Pt distribution throughout the total length of the channel, the flow direction was altered every 30 min.

(D) *Microstructured reactor/heat-exchanger*. The schematic view of this microreactor is shown in Fig. 3. The design procedure is discussed in Section 4 in detail.

Scanning electron microscopy was used to analyze the structure and thickness of the alumina layers

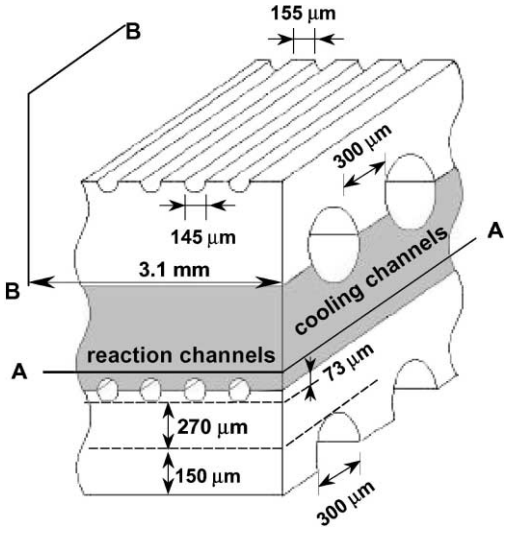

Fig. 3. Assembling of the aluminum microstructured reactor/heat-exchanger D: by stacking two plates, a set of reaction channels is produced. By adding the third one a set of cooling channels is produced. The region of numerical simulation is shown in gray. Planes A–A and B–B indicate the position at which the temperature distributions are shown in Fig. 8.

produced by the anodic oxidation. The process parameters for electrochemically prepared alumina films were optimized, with the goal to establish a basis for a direct, relatively easy and cheap way to produce alumina layers in microchannels. It was found that a uniform Al_2O_3 film was produced in a 10 wt.% oxalic acid solution at a density of the electric current of $15\,mA/cm^2$, confirming a good reproducibility of this technique. As an example, Fig. 4 shows a 25 μm thick alumina layer produced after oxidation for 2 h. Pt concentration in the alumina film was measured

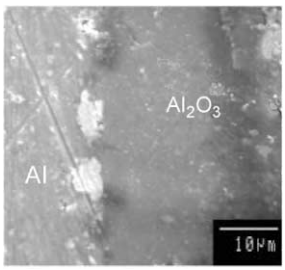

Fig. 4. SEM micrograph of the side view of the aluminum plate near the Al/Al_2O_3 interface after anodic oxidation in 10 wt.% oxalic acid for 2 h.

by energy-dispersive X-ray spectroscopy. Pt dispersion was determined by hydrogen chemisorption. Mean Pt crystallite sizes were determined from hydrogen chemisorption data by using site densities of $1.12 \times 10^{15}\,cm^{-2}$ of metal [15].

2.2. NH_3 oxidation runs

The microstructured reactors were tested in the NH_3 oxidation. The reactor feed streams consisted of 4–14 vol.% NH_3 in oxygen or oxygen/He mixture with inlet flow rates in the range 3000–5500 cm^3/min (STP). Analysis of reactants and products was performed by a on-line GC (HP 5890 series) equipped with Molsieve 5A and Porapak T columns and TCD detectors. The NO content of the effluent is calculated using a nitrogen mass balance. At temperatures below 280°C, when no NO was produced, the component mass balances were closed within 5%.

The catalytic reaction was ignited at a gas phase temperature of about 360°C by introducing a gas mixture into the reactor containing 8 vol.% NH_3, 22 vol.% O_2, and 70 vol.% He. An oxygen-depleted mixture was used to ignite the reaction, as the heat capacity of He is lower than that of oxygen. As a result, the ignition temperature of this mixture (360°C) is much lower than that of oxygen rich mixtures. After ignition, He was gradually replaced by oxygen and the temperature was set to the desired value. Prior to the kinetic experiments, the catalyst was positioned in a mixture of 6 vol.% NH_3 in oxygen at 325°C for about 12 h.

3. Results and discussion

3.1. Catalytic activity and selectivity

Prior to the kinetic study, the effects of the platinum loading, the reactor material, and the experimental conditions on selectivity were investigated to obtain the highest possible N_2O selectivity. As a starting point, the literature data for ammonia oxidation on a supported platinum catalyst were used. In these preliminary experiments, two different reactor materials and several catalysts with a different Pt loading were tested. Experiments were also performed to determine which NH_3/O_2 ratio and reaction temperature could give the highest N_2O selectivity.

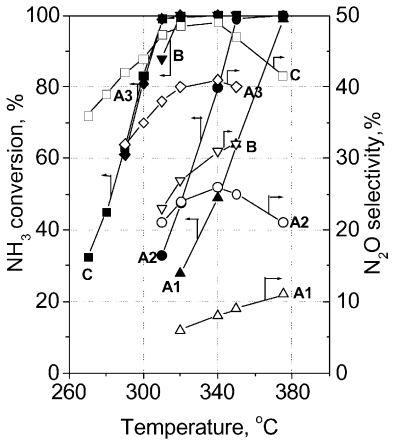

Fig. 5. Activity and selectivity to nitrous oxide of microstructured reactors A1, A2, A3, B, and C in the ammonia oxidation on Pt catalyst. Open symbols represent NH_3 conversion, closed symbols represent N_2O selectivity for the following microreactors: (▲,△) A1, (○,●) A2, (◇,◆) A3, (▼,▽) B, and (■,□) C. Reaction conditions: NH_3 6 vol.%, O_2 88 vol.%, balance-He. The flow velocity: 600, 1175, 4430, 580 and 4290 cm^3/min (STP) for microreactors A1, A2, A3, B, and C, respectively.

Fig. 5 compares the catalytic activities and selectivities of reactors A1, A2, A3, B, and C under the standard operating conditions. Four of these reactors have identical alumina support, and differ by the Pt loading and the geometry. It is clear that reactor C is the most active, as it completes NH_3 conversion at about 325°C, while reactor A1 is only starting to be active at this temperature and the activity curves of reactors A2 and A3 lie in between those of A1 and C. Maximum selectivity towards N_2O increases monotonously with increasing Pt loading up to 3.5 wt.%.

For proper evaluation, however, we should consider also the catalytic activity of a single Pt atom in these catalysts. Such comparison based on data of Fig. 6 reveals that reactors A1 and A2 show similar performances, with the calculated NH_3 consumption rate of about 20 s^{-1} at 300°C. However, reactors A3 and C remain considerably more active (TOF of about 40 s^{-1}) and reactor C yields the highest N_2O selectivity also. In order to rationalize the advantage of the catalysts in reactors A3 and C, we could compare the data on Pt dispersion in these catalysts. It is well known that Pt catalyzed ammonia oxidation is a structure sensitive reaction [13]. Therefore, the Pt cluster size plays an important role in the activity of these catalysts and also

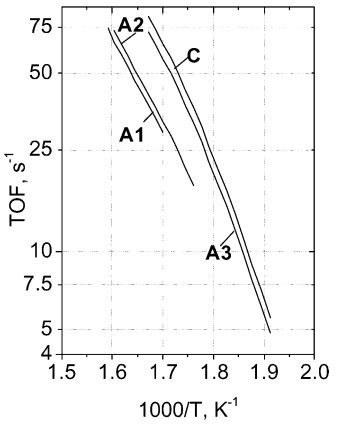

Fig. 6. Activity of microstructured reactors A1, A2, A3, and C per Pt atom in the ammonia oxidation. Reaction conditions: NH_3 6 vol.%, O_2 88 vol.%, balance-He, contact time: 0.51 ms.

it could have an influence on the product distribution by a great extend. According to the catalyst dispersion data (see Table 1), Pt exists as isolated atoms in the reactors A1 and A2, and it is present in the form of clusters in the reactors A3 and C. The formation of Pt clusters is believed to be responsible for the better performance of reactors A3 and C in the ammonia oxidation.

The data obtained on the supported catalysts were compared with those of reactor B which is a Pt monolith microreactor. As could be seen from Fig. 5, reactor B showed considerably lower nitrous oxide selectivity at the full conversion of ammonia as compared to reactors A3 and C. This could be explained based on the thermal behavior of those microreactor systems as will be presented in the following section.

3.2. Thermal behavior

The thermal profiles along the microchannels of the different microreactors were estimated using CFD calculations and a kinetic mechanism of the Pt catalyzed ammonia oxidation that is reported elsewhere [16]. Current understanding of the ammonia oxidation reaction for surface temperatures below 500°C is that NH_3 and oxygen after their adsorption on a surface form several active adspecies which react to form N_2, N_2O, and NO. In this mechanism nitrogen containing adspecies are assumed to occupy single "on-top" adsorption sites, and all other species occupy adsorption sites equivalent to that of oxygen [17].

A global analysis of the thermal behavior of the complete reactor module at the same power load of the furnace (W0) is presented in Table 2 and in Fig. 7. W1 represents the total heat of the reaction evolved during a test run. A relatively small part of this heat (W2) is consumed by heating the reaction mixture from the inlet temperature to the reaction temperature. The rest is removed via two routes, namely heat transfer via the four stainless steel screws (W3), connecting the reactor housing with the quench section, and heat loss to the environment (W4). Fig. 7 demonstrates the differences between the furnace and microreactor temperatures.

The smallest thermal resistance is clearly associated with microreactor C. Because of the excellent intrinsic heat conductivity of aluminum ($\lambda = 240\,W/m\,K$), the only significant heat transfer resistance in this case was located at the interface between the external microreactor wall and the nickel housing. In this case, the reactor temperature was equal to the furnace temperature at conversion of 7 vol.% NH_3. It is interesting to note that in this case all the heat produced by the oven was transferred to the environment.

For the Pt-monolith reactor B, due to the relatively low thermal conductivity of Pt ($\lambda = 72\,W/m\,K$) compared to that of aluminum, the heat generated inside the reaction channels cannot be transferred fast enough to the cooler. As a result, at the full conversion of 6 vol.% NH_3 a hot spot of about 25°C inside microreactor B can arise, which gives poor selectivity control.

Table 1
Characteristics of the platinum catalyst used in the microreactors

Microreactor	Pt mass (mg)	Al_2O_3 mass (mg)	Pt loading (wt.%)	Pt dispersion (%)	Mean platinum cluster size (Å)
A1	0.022	44	0.05	100	<9
A2	0.086	44	0.2	96	9
A3	0.560	44	1.3	48	19
C	0.543	16	3.5	40	23

Table 2
Thermal behavior of the complete reactor module[a]

NH_3 inlet concentration[b] (vol.%)	Furnace temperature (°C)	Heat released (W)		Heat consumed (W)		
		By furnace W0	By reactor W1	By reaction mixture W2[c]	By cooler W3[d]	By environment W4[e]
5	310	90	50	15	60	65
7	330	90	82	18	64	90
10	345	90	124	20	67	127
12	360	90	149	22	70	147

[a] Experiments were carried out on microreactor C.
[b] Total flow velocity was 5660 cm^3/min.
[c] Temperature of the inlet mixture was set at 177°C.
[d] Thermal conductivity of stainless steel was set at 16 W/m K, cooler temperature at −20°C.
[e] Calculated from the thermal balance over the system.

Although the geometry of the reactor is suitable to provide a high heat transfer rate, the thermal conductivity of the reactor material creates considerable heat transfer resistance. As a result, the maximum N_2O selectivity is considerably lower than in the case of the parallel plate reactor A3 due to considerable differences in the selectivities between the central and wall channels in reactor B.

As for the parallel plate reactor A, because of the excellent intrinsic heat conductivity of aluminum, the only significant heat transfer resistance in this case is due to the relatively small contact area between the catalyst plates and the nickel housing ($\lambda \approx 80$ W/m K). The result of a poor heat transfer was observed in the experiments with high ammonia concentrations. Several plates positioned in the middle of reactor A were melted when 12 vol.% NH_3 was used.

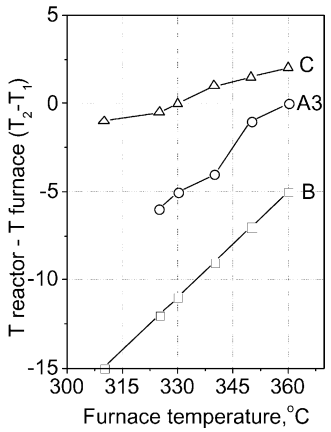

Fig. 7. The differences between the furnace and microreactor temperatures for the microstructured reactors A3, B, and C. The furnace load was kept at 90 W, the cooler was set at −20°C. The inlet NH_3 concentration was changed to provide a desired microreactor temperature (see Table 2).

Due to its better performance, the catalytic behavior of reactor C was further investigated by kinetic analysis, based on an extensive set of experimental runs which also included experiments at lower contact times, corresponding to feed flows in the range 2000–5500 cm^3/min (STP). The difference between furnace and microreactor temperatures did not exceed 5°C in all experiments. This allowed extension of the investigation to high NH_3 inlet concentrations and feed flow rates, both conditions being associated with large thermal loads. The kinetic parameters of the elementary reaction steps were determined by regression on integral data from 103 NH_3 oxidation runs over reactor C, with NH_3 conversion, and N_2 and N_2O selectivities as the experimental response. A simple isothermal plug-flow model was used to describe the flow in the microchannels. The data covered the effects of temperature, residence time, and inlet concentrations of both ammonia and oxygen. The regression procedure and the kinetic scheme are described in detail elsewhere [16].

It was found that decreasing the residence time to 0.3 ms had a positive influence on the N_2O selectivity. Furthermore, increasing the oxygen concentration to 90% gave two times more nitrous oxide than a stoichiometric NH_3/O_2 mixture. The significance of gas–solid interphase mass transfer limitations was

ruled out based on the calculation of the Damköhler number

$$Da = \frac{r_{NH_3} L_t d_h}{D_{NH_3} C_{NH_3}} \quad (1)$$

where r_{NH_3} is the measured turnover frequency of the ammonia oxidation on Pt, with $r_{NH_3} = 50\,s^{-1}$ at 573°C and 6 vol.% NH_3 in oxygen mixture, L_t the available amount of Pt active centers in alumina, $L_t = 7.5 \times 10^{-3}\,mol/m^2$, which corresponds to the Pt loading in alumina of 3.5 wt.%, d_h the hydraulic diameter of the channels in the microreactor, $d_h = 2.8 \times 10^{-4}\,m$, D_{NH_3} the diffusivity of NH_3 in oxygen, C_{NH_3} the ammonia concentration in mol/m^3. It was found that $Da < 0.3$ at all reaction conditions where temperature was below 300°C. This indicates that the mass transfer in the channels of the microreactor was always much greater than the reaction rate, thus diffusion limitations can be neglected. However, the Damköhler number became of the order of unity for reaction temperatures exceeding 325°C. In this case diffusion limitation was considered by using the computational fluid dynamics Fluent® code, when modeling the microreactor operated under non-isothermal conditions, such as those adopted in the kinetic study on microreactor C [16].

According to our experimental observation, microreactor C operated autothermally at 325°C with 14 vol.% NH_3 in the inlet mixture. Thus, further increase in the NH_3 concentration would also increase the temperature while decreasing the N_2O selectivity. Therefore, to operate a microreactor with maximum selectivity at such conditions, a cross flow design was adopted to increase the surface that is available for heat-exchange. This design was realized in the externally cooled microreactor/heat-exchanger D.

4. Geometry design and model development of a cross flow microreactor/heat-exchanger

4.1. Geometry design

To avoid external diffusion limitation in the whole range of the reaction conditions (both temperatures of 250–350°C and local ammonia concentration up to 15 vol.%), the hydraulic diameter of the reaction channels was set at 145 μm in the microreactor/heat-exchanger. Based on the experimental data, the length of the reaction channels was fixed at 6.5×10^{-3} m to provide an optimal contact time of 0.33 ms at linear flow velocity of 20 m/s. Estimation of the pressure drop across the microreactor channel, according to the expression for an empty tube (2), gives the difference between the reactor inlet and outlet of about 3.5%

$$\Delta p = 32 \frac{\Delta l \bar{\upsilon}_x \mu}{d_h^2} \quad (2)$$

In Eq. (2), Δl represents the microchannel length, υ_x the average linear velocity, and μ is viscosity of the reaction mixture. The Reynolds number of 220 confirms the laminar flow mode in the reaction microchannels.

From a practical point of view, it is desirable that a single microreactor plate has a square shape. Thus, the width of a plate was also fixed at 6.5×10^{-3} m. Within this distance 20 reaction channels with the hydraulic diameter of 145 μm were machined at equal distances from each other. To provide enough coolant at full conversion of 15 vol.% NH_3 to N_2 and N_2O with a 1:1 ratio, the diameter and number of cooling channels were also optimized. In this estimation, the linear flow velocity of the reaction mixture was set at 20 m/s, outlet temperatures of the coolant and outlet gas mixture were fixed at 325°C, and nitrogen at 20°C was supposed to be the coolant. It was also assumed that before entering the microreactor, the inlet reaction mixture was preheated to 177°C. It was found that nine channels of 300 μm in diameter could provide enough coolant at a linear velocity of 35 m/s. This gives a pressure drop of 1.5%, corresponding to *Re* number of 930 at the channel outlet. Thus, the coolant flow is also laminar. A set of reaction channels in one plate is separated by an aluminum layer from a set of the cooling channels. To provide enough durability of a single microreactor plate, the distance between the reaction and cooling channels was set at 270 μm.

4.2. Computational domain

The geometry of the microreactor/heat-exchanger was laid out using the grid generator preBFC, with the geometry specifications described in the previous section. The initial boundary mesh for the geometry was created using preBFC to first distribute nodes on all boundary curves at an average density

of 16 nodes/mm. A structured, two-dimensional surface mesh was created on all boundary surfaces. The surface mesh was then extruded in the direction parallel to the cooling channels to generate a structured three-dimensional mesh throughout the reactor volume. For this case, a total of 132,000 elements were used. Finally, a set of 20 reaction half channels was made with a 90° rotation relative to the position of the cooling channels. The geometry of the reaction channels was chosen in accordance with the grid obtained, to keep the total number of computational elements to a minimum. An assumption was made that the flow in the channels is symmetrical relative to the center of the channel, therefore only half of the region of each channel is simulated.

The Fluent® code was used to calculate gas-phase and surface temperatures, and velocity and mole fraction profiles in case of a surface reaction of ammonia oxidation on Pt. Fluent® uses the control-volume-finite-element method [18] to solve the conservation equations for mass, momentum, and energy. The equations were solved using the SIMPLEC algorithm.

The simulation was based on the 3D geometry of a single reactor plate. About 20 h of CPU time (CRAY Origin 2000 supercomputer) were needed for solution convergence. In order to determine convergence, a criterion of 10^{-4} was used for each velocity component, a criterion of 10^{-3} for pressure, and of 10^{-7} for enthalpy and chemical species concentrations. Residuals for each iteration were normalized vs residual values obtained after the second iteration of the solver. The number of nodes in the mesh was doubled until an average velocity difference of less then 5% was achieved for two successive meshes. The lower node density was then used to generate the computational mesh for the reactor D.

4.3. Inlet and boundary conditions

Calculations were performed with cross flow of the reaction mixture containing 20 vol.% NH_3 in O_2 at an inlet temperature of 250°C in one passage, and cold N_2 of 20°C in the other passage. A constant heat flux to the environment was set at the wall located at the coolant outlet. The remaining outer walls were considered to be adiabatic. The inner walls of the cooling channels and the walls between channels were considered as conducting walls with a heat conductivity of aluminum which is equal to 230 W/m K. The inner walls of the reaction channels were considered as conducting walls with a heat conductivity of alumina which is equal to 1.0 W/m K. The thickness of this walls was 25 μm. The areas produced by intersecting the planes through the centers of the microchannels were defined to be planes of symmetry (which is equivalent to zero gradient conditions). The operating pressure was set at 101.3 kPa at the channel outlets. The chemical reaction (3) on the surface of the reaction channels was used as a boundary condition for chemical species

$$2NH_3 + 1.75O_2 \rightarrow 0.5N_2 + 0.5N_2O + 3H_2O + 593\,\text{kJ} \quad (3)$$

Thus, the detailed mechanism of ammonia oxidation was not used here and an adopted power law form (4) of the rate expression was used instead for temperature profile calculations. This was done based on the analysis of selectivities to N_2 and N_2O and the reaction orders in ammonia and oxygen and the apparent activation energy obtained on microreactor C in the temperature range of 310–340°C.

$$r_{NH_3} = \frac{k_1 k_2 p_{NH_3}}{(1 + k_1 p_{NH_3}) p_{O_2}^{0.06}} \quad (4)$$

Eq. (4) includes two kinetic parameters with an Arrhenius temperature dependence k_1 and k_2. The strong correlation between the activation energies E_1 and E_2 made it not possible to estimate the individual parameters. Therefore, the parameter k_1 was fixed at $9.13 \times 10^2\,\text{atm}^{-1}$ in the selected temperature range and the activation energy and the pre-exponent factor of parameter k_2 (72.3 kJ/mol, $1.46 \cdot 10^8\,\text{s}^{-1}\,\text{atm}^{0.06}$) were found by regression on data from ammonia oxidation runs, with ammonia conversion as the experimental response.

4.4. Results of numerical simulations

In order to assess the validity of the simulation results, a comparison between the simulated pressure drop and an empty tube correlation (2) is made. For the fluid properties and module geometry described in previous sections and an inlet velocity of 35 m/s in the cooling channels, the pressure drop of 3500 Pa was

observed in the simulations. This is in a good agreement with the estimation made in Section 4.1. Pressure drop data was also obtained from the simulations corresponding to lower and higher Reynolds numbers in the range of 200–1800. A good agreement was also observed for the investigated range of velocities in the cooling channels. The simulation data falls within 5% of the value obtained from correlation (2). This level of agreement, over almost one order of magnitude of *Re* numbers, provides considerable support of the simulation results.

Velocity profiles were also obtained from the simulations performed at different *Re* numbers. For $Re = 200$, profiles look qualitatively identical to those shown for $Re = 1000$. At larger flows as well, the velocity contours are essentially similar to those obtained at lower Reynolds number, with entrance effects considerably more persistent with increasing the Reynolds number. The velocity distribution reflects the temperature profile through the equation of state, which was used to model the temperature dependence of the mixture density. The fluid flow velocity is increased by the gas expansion as the gas mixture passes over the hot reactor.

The temperature profiles at the plane A–A positioned inside the alumina layer and at the plane B–B (see Fig. 3) are shown in Fig. 8. In this simulation, a simplification was made that the channel cross sections of all channels of a passage are exposed to a uniform flow. The average temperatures of the reaction channels are different and depend on their positions with respect to the coolant inlet. The increase of the coolant temperature results in a progressive increase in the temperature of the catalyst wall in the reaction channels, which are positioned further away from the coolant inlet. For the 19th and 20th reaction channels this effect is compensated by the heat loss to the environment. The temperature profiles at the position of cooling channels look qualitatively identical to those observed for the plane corresponding to the reaction channels. However, the difference between hot spot and cold spot temperatures becomes smaller by 3°C.

In general, the cross flow design of the microreactor provides a relatively small difference in catalyst temperature of 9°C, improving the overall selectivity to a desired product for reaction conditions corresponding to an adiabatic temperature rise of about 1400°C. On the other hand, the present work

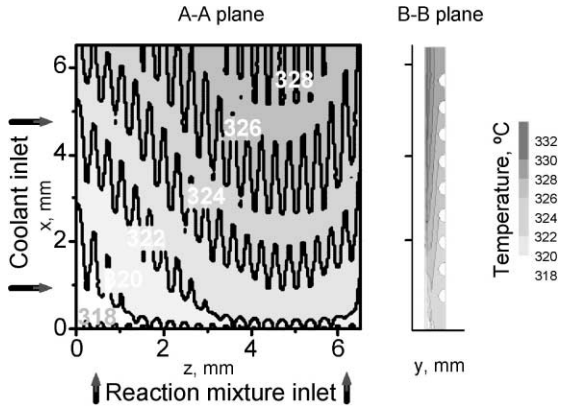

Fig. 8. Cross-sectional temperature profiles at the planes positioned inside the alumina layer (A–A, see Fig. 3) and through reaction channel No. 11 perpendicular to the cooling channels (B–B). Ammonia conversion: 75%. Inlet mixture: 20 vol.% NH_3 in oxygen. Reagent linear flow velocity: 20 m/s, coolant flow velocity: 35 m/s, inlet temperatures: reagents 177°C, coolant 20°C. Arrows show the flow directions.

demonstrates also some aspects of the reactor design which require further development. In the present design, the difference in temperature between different reaction channels gives a difference in the ammonia conversion as large as 20%. That could be unacceptable for a detailed kinetic study. So, the future design work is aimed at minimizing such temperature differences by introducing a non-uniform coolant distribution in the cooling channels, e.g. optimizing the heat-exchange rate between two sets of channels.

5. Conclusions

We have showed that both the intrinsic conductivity of the reactor material and the geometry of the microreactor are crucial to provide near-isothermal conditions inside a microreactor. A microstructured reactor, made with highly conductive metals and connected to a quench section via reasonably thick metallic screws, has practically the same reaction conditions in all microchannels. This leads to an even reaction rate and considerable increase in selectivity to a desired product. With very high reagent

concentrations, a cross flow microreactor/heat-exchanger could provide almost isothermal conditions improving overall selectivity. The aluminum-based microreactor/heat-exchanger shows temperature differences less than 6°C along the axial coordinate, and negligible temperature differences between microchannels along the transverse coordinate (4°C), for reaction conditions corresponding to an adiabatic temperature rise of about 1400°C. Obviously, such systems could afford new opportunities for improvement of existing gas/solid catalytic processes with strongly exothermic reactions. The use of this type of integrated microreactor also makes it possible to estimate the intrinsic kinetic rate of the reaction, because mass transfer limitation is eliminated.

References

[1] Proceedings of the Fourth International Conference on Microreaction Technology, IMRET 4, March 5–9, 2000, Atlanta, USA.
[2] R. Srinivasan, I.M. Hsing, J.F. Ryley, M.P. Harold, K.F. Jensen, M.A. Schmidt, Micromachined chemical reactors for surface catalyzed oxidation reactions, in: Proceedings of the Seventh IEEE Solid State Sensor and Actuator Workshop, Hilton Head Island, South Carolina, June 3–6, 1996, pp. 15–18.
[3] W. Ehrfeld, V. Hessel, H. Mobius, Th. Richter, K. Russow, Potentials and Realization of Microreactors, Dechema Monographs, Vol. 132, VCH Verlagsgesellschaft, 1996, pp. 1–28.
[4] A. Cybulski, J. Moulijn, Structured Catalysts and Reactors, Dekker (Marcel), New York (Basel), 1997.
[5] V. Ragaini, G. De Luca, B. Ferrario, P. Della Porta, Chem. Eng. Sci. 35 (1980) 2311.
[6] A. Cybulski, J. Moulijn, Catal. Rev. Sci. Eng. 36 (1994) 179.
[7] A. Cybulski, J. Moulijn, Chem. Eng. Sci. 49 (1994) 19.
[8] G. Groppi, E. Tronconi, Chem. Eng. Sci. 55 (2000) 2161.
[9] T. Ioannides, X.E. Verykios, Catal. Today 46 (1998) 71.
[10] R. Srinivasan, I.M. Hsing, P.E. Berger, M.P. Harold, J.F. Ryley, J.J. Lerou, K.F. Jensen, AIChE J. 43 (1997) 3059.
[11] I.M. Hsing, R. Srinivasan, M.P. Harold, K.F. Jensen, M.A. Schidt, Chem. Eng. Sci. 55 (2000) 3.
[12] E. Tronconi, G. Groppi, Chem. Eng. Sci. 55 (2000) 6021–6036.
[13] J.J. Ostermaier, J.R. Katzer, W.H. Manogue, J. Catal. 41 (1976) 277.
[14] E.V. Rebrov, G.B.F. Seijger, H.P.A. Calis, M.H.J.M. de Croon, C.M. van den Bleek, J.C. Schouten, Appl. Catal. A 206 (2001) 125.
[15] L. Spenadel, M. Boudart, J. Phys. Chem. 64 (1960) 204.
[16] E.V. Rebrov, M.H.J.M. de Croon, J.C. Schouten, Development of the kinetic model for platinum catalyzed ammonia oxidation in a microreactor, Chem. Eng. J. (submitted for publication).
[17] J.M. Bradley, A. Hopkinson, D.A. King, J. Phys. Chem. 99 (1995) 17032.
[18] B.R. Baliga, S.V. Patankar, Numer. Heat. Transfer 6 (1983) 245.